Complement Factor H Polymorphism in Age-Related Macular Degeneration

Robert J. Klein, *et al.*

Science **308**, 385 (2005);
DOI: 10.1126/science.1109557

qualitative, and it is still possible that these pathways have a quantitative influence on the epidermal barrier wound response.

References and Notes

1. A. J. Nappi, E. Ottaviani, *Bioessays* **22**, 469 (2000).
2. H. G. Boman, D. Hultmark, *Annu. Rev. Microbiol.* **41**, 103 (1987).
3. M. J. Galko, M. A. Krasnow, *PLoS Biol.* **2**, E239 (2004).
4. P. N. Walsh, S. S. Ahmad, *Essays Biochem.* **38**, 95 (2002).
5. J. A. Hoffmann, J. M. Reichhart, *Nat. Immunol.* **3**, 121 (2002).
6. S. Thoma-Uszynski *et al.*, *Science* **291**, 1544 (2001).
7. N. Silverman, T. Maniatis, *Genes Dev.* **15**, 2321 (2001).
8. P. Martin, *Science* **276**, 75 (1997).
9. W. Wood *et al.*, *Nat. Cell Biol.* **4**, 907 (2002).
10. M. Ramet, R. Lanot, D. Zachary, P. Manfruelli, *Dev. Biol.* **241**, 145 (2002).
11. A. Jacinto, A. Martinez-Arias, P. Martin, *Nat. Cell Biol.* **3**, E117 (2001).
12. L. Kockel, J. G. Homsy, D. Bohmann, *Oncogene* **20**, 2347 (2001).
13. S. Werner, R. Grose, *Physiol. Rev.* **83**, 835 (2003).
14. G. Li *et al.*, *Dev. Cell* **4**, 865 (2003).
15. E. B. Lewis, *Nature* **276**, 565 (1978).
16. G. Struhl, *J. Embryol. Exp. Morphol.* **76**, 297 (1983).
17. A. Macias, G. Morata, *EMBO J.* **15**, 334 (1996).
18. E. L. Wiellette *et al.*, *Development* **126**, 5373 (1999).
19. T. R. Wright, *J. Hered.* **87**, 175 (1996).
20. J. Schaefer *et al.*, *Science* **235**, 1200 (1987).
21. Materials and methods are available as supporting material on *Science* Online.
22. S. B. Scholnick, S. J. Bray, B. A. Morgan, C. A. McCormick, J. Hirsh, *Science* **234**, 998 (1986).
23. L. Chen *et al.*, *MOD* **114**, 95 (2002).
24. K. A. Mace, J. C. Pearson, W. McGinnis, data not shown.
25. S. J. Bray, F. C. Kafatos, *Genes Dev.* **5**, 1672 (1991).
26. A. E. Uv, E. J. Harrison, S. J. Bray, *Mol. Cell. Biol.* **17**, 6727 (1997).
27. C. Nusslein-Volhard, E. Wieschaus, H. Kluding, *Rouxs Arch. Dev. Biol.* **193**, 267 (1984).
28. S. Ostrowski, H. A. Dierick, A. Bejsovec, *Genetics* **161**, 171 (2002).
29. J. Hemphala, A. Uv, R. Cantera, S. Bray, C. Samakovlis, *Development* **130**, 249 (2003).
30. H. Lee, P. N. Adler, *Mech. Dev.* **121**, 37 (2004).
31. S. Barolo, B. Castro, J. W. Posakony, *Biotechniques* **36**, 436 (2004).
32. B. K. Dieckgraefe, D. M. Weems, *Am. J. Physiol.* **276**, G322 (1999).
33. G. J. Liaw *et al.*, *Genes Dev.* **9**, 3163 (1995).
34. M. Ashida, P. T. Brey, *Proc. Natl. Acad. Sci. U.S.A.* **92**, 10698 (1995).
35. K. Venkatesan, H. R. McManus, C. C. Mello, T. F. Smith, U. Hansen, *Nucleic Acids Res.* **31**, 4304 (2003).
36. T. Wilanowski *et al.*, *Mech. Dev.* **114**, 37 (2002).
37. S. B. Ting *et al.*, *Biochem. J.* **370**, 953 (2003).
38. E. I. Kudryavtseva *et al.*, *Dev. Dyn.* **226**, 604 (2003).
39. S. B. Ting *et al.*, *Nat. Med.* **9**, 1513 (2003).
40. S. B. Ting *et al.*, *Science* **308**, 411 (2005).

41. We thank S. Jane for communication of unpublished results, A. Tugores for the *Ddc* genomic clone, O. Drivenes for enhancer stains, and M. Ronshaugen for rhodamine-dextran injections and manuscript suggestions. L. Chen, R. Hodgetts, S. Barolo, J. Posakony, S. Wasserman, and T. Ip provided materials, and D. Kosman helped with confocal microscopy. W.M. is funded by R01HD28315, and J.C.P. is funded by T32GM07240.

Supporting Online Material

www.sciencemag.org/cgi/content/full/308/5720/381/DC1
Materials and Methods
Figs. S1 to S3
References and Notes

16 November 2004; accepted 26 January 2005
10.1126/science.1107573

Complement Factor H Polymorphism in Age-Related Macular Degeneration

Robert J. Klein,[1] Caroline Zeiss,[2]* Emily Y. Chew,[3]* Jen-Yue Tsai,[4]* Richard S. Sackler,[1] Chad Haynes,[1] Alice K. Henning,[5] John Paul SanGiovanni,[3] Shrikant M. Mane,[6] Susan T. Mayne,[7] Michael B. Bracken,[7] Frederick L. Ferris,[3] Jurg Ott,[1] Colin Barnstable,[2] Josephine Hoh[7]†

Age-related macular degeneration (AMD) is a major cause of blindness in the elderly. We report a genome-wide screen of 96 cases and 50 controls for polymorphisms associated with AMD. Among 116,204 single-nucleotide polymorphisms genotyped, an intronic and common variant in the complement factor H gene (*CFH*) is strongly associated with AMD (nominal P value $<10^{-7}$). In individuals homozygous for the risk allele, the likelihood of AMD is increased by a factor of 7.4 (95% confidence interval 2.9 to 19). Resequencing revealed a polymorphism in linkage disequilibrium with the risk allele representing a tyrosine-histidine change at amino acid 402. This polymorphism is in a region of CFH that binds heparin and C-reactive protein. The *CFH* gene is located on chromosome 1 in a region repeatedly linked to AMD in family-based studies.

Age-related macular degeneration (AMD) is the leading cause of blindness in the developed world. Its incidence is increasing as the elderly population expands (*1*). AMD is characterized by progressive destruction of the retina's central region (macula), causing central field visual loss (*2*). A key feature of AMD is the formation of extracellular deposits called drusen concentrated in and around the macula behind the retina between the retinal pigment epithelium (RPE) and the choroid. To date, no therapy for this disease has proven to be broadly effective. Several risk factors have been linked to AMD, including age, smoking, and family history (*3*). Candidate-gene studies have not found any genetic differences that can account for a large proportion of the overall prevalence (*2*). Family-based whole-genome linkage scans have identified chromosomal regions that show evidence of linkage to AMD (*4*–*8*), but the linkage areas have not been resolved to any causative mutations.

Like many other chronic diseases, AMD is caused by a combination of genetic and environmental risk factors. Linkage studies are not as powerful as association studies for the identification of genes contributing to the risk for common, complex diseases (*9*). However, linkage studies have the advantage of searching the whole genome in an unbiased manner without presupposing the involvement of particular genes. Searching the whole genome in an association study requires typing 100,000 or more single-nucleotide polymorphisms (SNPs) (*10*). Because of these technical demands, only one whole-genome association study, on susceptibility to myocardial infarction, has been published to date (*11*).

Study design. We report a whole-genome case-control association study for genes involved in AMD. To maximize the chance of success, we chose clearly defined phenotypes for cases and controls. Case individuals exhibited at least some large drusen in a quantitative photographic assessment combined with evidence of sight-threatening AMD (geographic atrophy or neovascular AMD). Control individuals had either no or only a few small drusen. We analyzed our data using a statistically conservative approach to correct for the large number of SNPs tested, thereby guaranteeing that the probability of a false positive is no greater than our reported P values.

We used a subset of individuals who participated in the Age-Related Eye Disease Study (AREDS) (*12*). From the AREDS

[1]Laboratory of Statistical Genetics, Rockefeller University, 1230 York Avenue, New York, NY 10021, USA. [2]Department of Ophthalmology and Visual Science, Yale University School of Medicine, 330 Cedar Street, New Haven, CT 06520, USA. [3]National Eye Institute, Building 10, CRC, 10 Center Drive, Bethesda, MD 20892–1204, USA. [4]Biological Imaging Core, National Eye Institute, 9000 Rockville Pike, Bethesda, MD 20892, USA. [5]The EMMES Corporation, 401 North Washington Street, Suite 700, Rockville MD 20850, USA. [6]W. M. Keck Facility, Yale University, 300 George Street, Suite 201, New Haven, CT 06511, USA. [7]Department of Epidemiology and Public Health, Yale University School of Medicine, 60 College Street, New Haven, CT 06520, USA.

*These authors contributed equally to this work.
†To whom correspondence should be addressed. E-mail: josephine.hoh@yale.edu

sample, we identified 96 case subjects and 50 control subjects as described (*13*). Because there can be many precursors to the development of either geographic atrophy or choroidal neovascularization, we purposely selected the group of study participants who had both large drusen and sight-threatening AMD as cases. All individuals identified themselves as "white, not of Hispanic origin." To the extent possible, we kept the proportions of males/females and smokers/nonsmokers the same in cases and controls. Controls were purposely chosen to be older than the cases to increase the probability that they would remain without AMD (table S1).

All 146 individuals were genotyped as described (*13*). A summary of genotyping quality can be found in table S2. Of the 116,204 SNPs genotyped, 105,980 both were informative and passed our quality-control checks. We then proceeded to analyze the 103,611 of these SNPs that lie on the 22 autosomal chromosomes.

Single-marker associations. For each SNP, we tested for allelic association with disease status. To account for multiple testing, we used the Bonferroni correction and considered significant only those SNPs for which $P < 0.05/103{,}611 = 4.8 \times 10^{-7}$. This correction is known to be conservative and thus "overcorrected" the raw P values (*14*). Of the autosomal SNPs, only two, rs380390 and rs10272438, are significantly associated with disease status (Bonferroni-corrected $P = 0.0043$ and $P = 0.0080$, respectively) (Fig. 1A).

One criticism of case-control association studies such as ours is that population stratification can result in false-positive results. If the cases and controls are drawn from populations of different ancestry, with different allele frequencies, we might detect these population differences instead of loci associated with the disease. All individuals in this study self-identify their ethnicity as non-Hispanic white, and all of the case and control individuals are drawn from the same AREDS population. There was some differential recruiting of cases from office practices and recruiting of controls from radio and newspaper advertising (*3*). Finding two SNPs out of >100,000 implied the absence of genetic stratification, but we nonetheless used genomic control methods to control for this possibility (*15*). We consistently found that the significance of the tests was not inflated and that, therefore, these two SNPs are significantly associated with disease.

SNP rs380390 was successfully genotyped in all individuals. In 21 individuals, no genotype was determined for SNP rs10272438, and it appears to be excessively out of Hardy-Weinberg equilibrium (HWE $\chi^2 = 36$), indicating possible genotyping errors. Missing genotypes were determined by resequencing (*16*). After inclusion of these additional genotypes, the association was no longer significant after Bonferroni correction. Furthermore, the SNP with the third-lowest P value, rs1329428 (Bonferroni-corrected $P = 0.14$), is located 1.8 kb telomeric to rs380390. The genotype frequencies at these two neighboring loci vary between the case and control populations (Fig. 1B). Homozygotes for the C allele of rs380390 and the C allele at rs1329428 have an increased risk of developing AMD (Table 1). The risk conferred by these genotypes accounts for approximately 45% (rs380390) to 61% (rs1329428) of the total population risk (Table 1). We therefore focused on these two SNPs.

Risk haplotype. These two SNPs lie in an intron of the gene for complement factor H (*CFH*), located on chromosome 1q31 (GenBank accession NM_000186). Because both SNPs are noncoding and neither appears to alter a conserved sequence, we explored whether the two SNPs are in linkage disequilibrium with a functional polymorphism. Analysis of linkage disequilibrium throughout this chromosomal region (Fig. 2A) revealed that the two SNPs lie in a 500-kb region of high linkage disequilibrium. Because this region is longer than typically observed blocks of high linkage disequilibrium (*17*) and there are long stretches in this region where there are no SNPs in our data set (Fig. 2B), we referred to other data sources with denser SNP coverage to narrow the region.

We used data from the International HapMap project to look at patterns of linkage disequilibrium in a population of residents of Utah with ancestry from northern and western

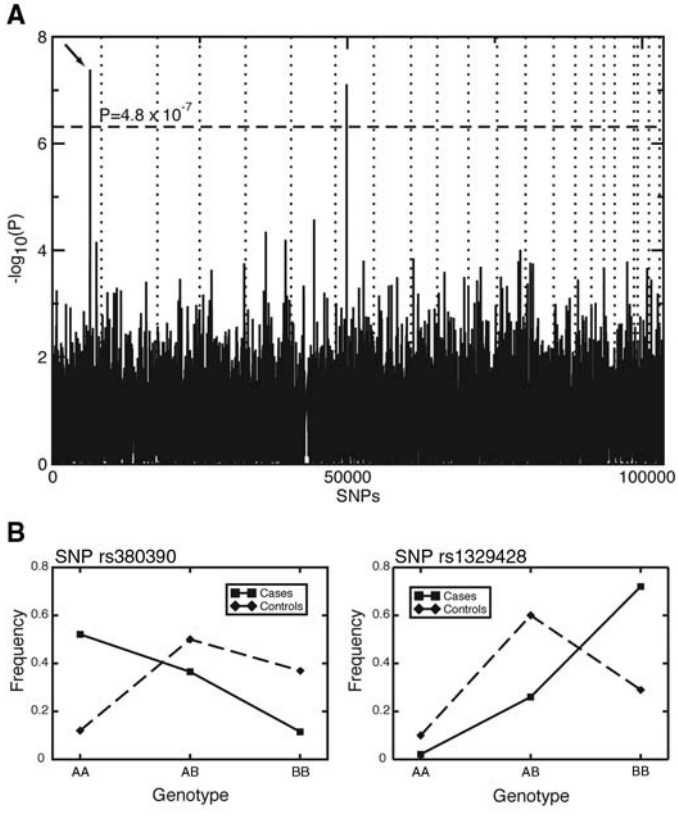

Fig. 1. (**A**) P values of genome-wide association scan for genes that affect the risk of developing AMD. $-\log_{10}(p)$ is plotted for each SNP in chromosomal order. The spacing between SNPs on the plot is uniform and does not reflect distances between SNPs on the chromosomes. The dotted horizontal line shows the cutoff for $P = 0.05$ after Bonferroni correction. The vertical dotted lines show chromosomal boundaries. The arrow indicates the peak for SNP rs380390, the most significant association, which was studied further. (**B**) Variation in genotype frequencies between cases and controls.

Table 1. Odds ratios and population attributable risks (PARs) for AMD. The dominant odds ratio and PAR compare the likelihood of AMD in individuals with at least one copy of the risk allele versus individuals with no copy of the risk allele. The recessive odds ratio and PAR compare the likelihood of AMD in individuals with two copies of the risk allele versus individuals with no more than one copy of the risk allele. The population frequencies for the risk genotypes are taken from the CEU HapMap population (CEPH collection of Utah residents of northern and western European ancestry).

Attribute	rs380390 (C/G)	rs1329428 (C/T)
Risk allele	C	C
Allelic association χ^2 nominal P value	4.1×10^{-8}	1.4×10^{-6}
Odds ratio (dominant) (95% CI)	4.6 (2.0–11)	4.7 (1.0–22)
PAR (95% CI)	70% (42–84%)	80% (0–96%)
Frequency in HapMap CEU	0.70	0.82
Odds ratio (recessive) (95% CI)	7.4 (2.9–19)	6.2 (2.9–13)
PAR (95% CI)	46% (31–57%)	61% (43–73%)
Frequency in HapMap CEU	0.23	0.41

Europe [the Centre d'Étude du Polymorphisme Humain (CEPH) sample] (*18*). In the 500-kb region of interest, there were only 19 SNPs in our data set as compared with 152 SNPs in the HapMap data set. Using a standard definition of linkage-disequilibrium blocks (*17*), we found that the two associated SNPs lie in a block that is 41 kb long and entirely contained within the *CFH* gene (Fig. 2C).

Six SNPs from our data set were in this 41-kb region. These SNPs form four predominant haplotypes, each with a frequency greater than 1% (table S3). Combined, these four haplotypes represent 99% of the chromosomes in this study. Reconstructing inferred haplotypes and building a phylogenetic tree allowed assessment of the evolutionary relationship between haplotypes (Fig. 2D). Using inferred haplotypes for each individual, we computed the odds ratio of the risk for disease in a nested cladistic framework under both dominant and recessive models (*19*). The highest risk was conferred by haplotype N1, which is the only haplotype containing the risk allele at SNP rs380390. Being heterozygous for this haplotype increases the likelihood for AMD by a factor of 4.6 [95% confidence interval (CI) 2.0 to 11] in our sample population. Being homozygous for this haplotype increases the likelihood for AMD by a factor of 7.4 (95% CI 3.0 to 19) in our sample population. Therefore, we expected to find the functionally relevant polymorphism in the context of haplotype N1. Most likely, this polymorphism would occur somewhere in the *CFH* gene, because the 41-kb haplotype block is entirely within *CFH*.

From markers to candidate functional polymorphism. To identify the polymorphism underlying susceptibility to AMD, we chose 96 individuals for exonic resequencing, including the exon/intron junctions. We sequenced all *CFH* exons, including those outside of the 41-kb block, as well as the region of SNP rs380390 as a control. SNP rs380390 was successfully resequenced in 93 individuals; the genotype derived from resequencing matched the original genotype in all cases. We identified a total of 50 polymorphisms; 17 of these have a minor-allele frequency of at least 5% (table S4). Of these 17, three represent nonsynonymous polymorphisms. We found a polymorphism in exon 9 of *CFH* (rs1061170) that is located 2 kb upstream of the 41-kb haplotype block, represents a tyrosine-histidine change, and is the polymorphism most strongly associated with AMD among the nonsynonymous SNPs we found. Adding this

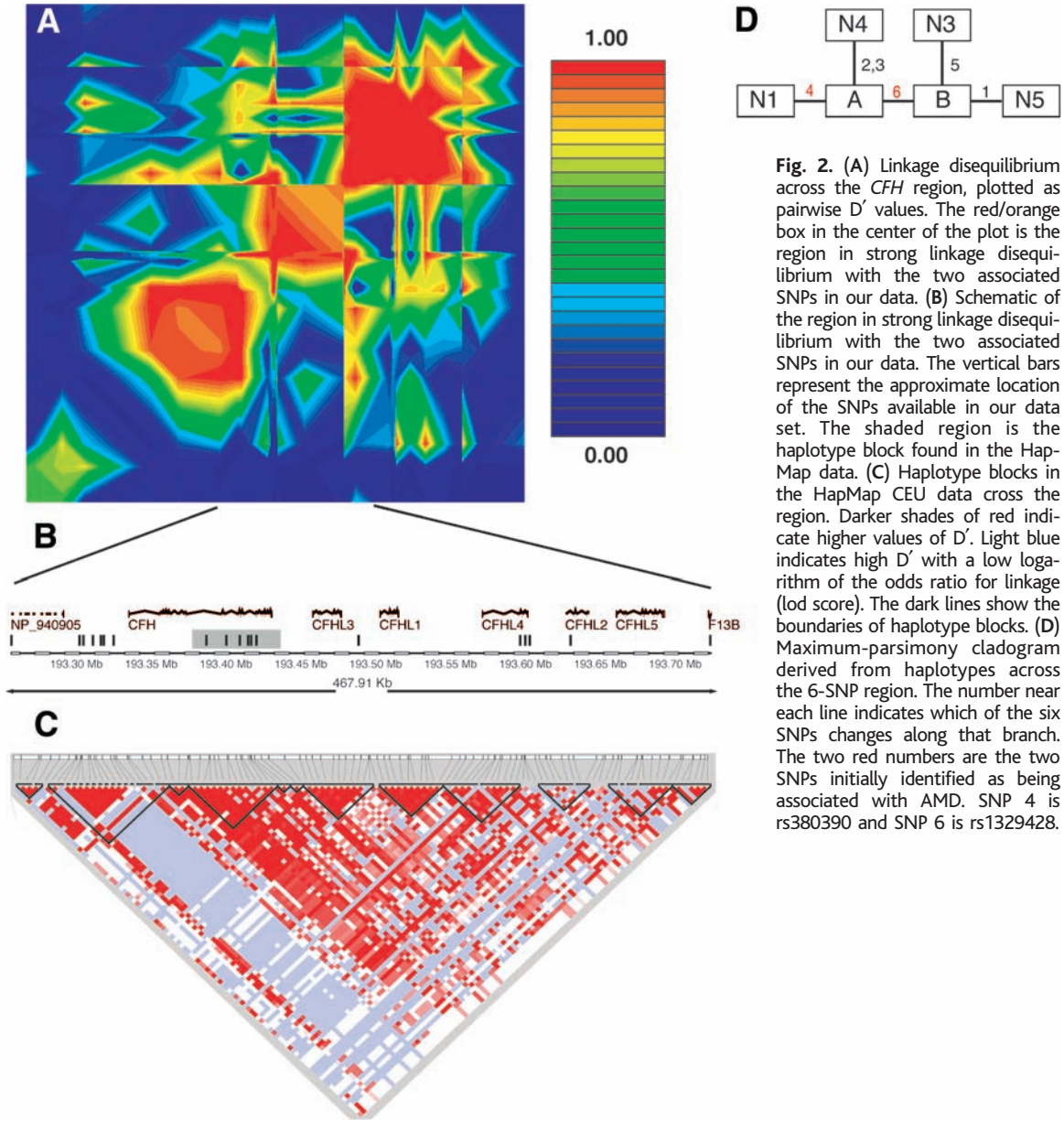

Fig. 2. (**A**) Linkage disequilibrium across the *CFH* region, plotted as pairwise D′ values. The red/orange box in the center of the plot is the region in strong linkage disequilibrium with the two associated SNPs in our data. (**B**) Schematic of the region in strong linkage disequilibrium with the two associated SNPs in our data. The vertical bars represent the approximate location of the SNPs available in our data set. The shaded region is the haplotype block found in the HapMap data. (**C**) Haplotype blocks in the HapMap CEU data cross the region. Darker shades of red indicate higher values of D′. Light blue indicates high D′ with a low logarithm of the odds ratio for linkage (lod score). The dark lines show the boundaries of haplotype blocks. (**D**) Maximum-parsimony cladogram derived from haplotypes across the 6-SNP region. The number near each line indicates which of the six SNPs changes along that branch. The two red numbers are the two SNPs initially identified as being associated with AMD. SNP 4 is rs380390 and SNP 6 is rs1329428.

SNP to the haplotype analysis reveals that 97% of the chromosomes with the highest risk haplotype (N1) also have the risk allele (His).

Human complement factor H. Several lines of evidence support the hypothesis that sequence polymorphisms in *CFH* can lead to AMD. First, the gene for *CFH* is located on chromosome 1q31, a region that had been implicated in AMD by six independent linkage scans (*4*–*8*, *20*). Although one study concluded that mutations in a different gene in this region (*HEMICENTIN-1*) were responsible for AMD (*20*), mutations in *HEMICENTIN-1* have not been found to be generally associated with AMD in three separate, independent studies (*7*, *21*, *22*).

CFH is a key regulator of the complement system of innate immunity (*23*). The complement system protects against infection and attacks diseased and dysplastic cells and normally spares healthy cells. When C3 convertase is activated, it leads to the production of C3a and C3b and then to the terminal C5b-9 complex. CFH on cells and in circulation regulates complement activity by inhibiting the activation of C3 to C3a and C3b and by inactivating existing C3b.

Various components of the complement cascade, including the C5b-9 complex, have been identified in the drusen of patients with AMD (*24*, *25*). We also examined the eyes of four patients with AMD to look for the presence of C5b-9 (fig. S1). Deposition of activated complement C5b-9 was noted in Bruch's membrane, in the intercapillary pillars, and within drusen. The observation of complement components in drusen in both humans (*24*, *25*) and mice (*26*) has led to the hypothesis that AMD results from an aberrant inflammatory process that includes inappropriate complement activation (*27*).

Both age and smoking, two important risk factors for AMD, influence plasma levels of complement factor H (*28*). *CFH* sequences have been observed in an expressed sequence tag library derived from human RPE and choroid (*29*). We confirmed by immunofluorescence experiments that CFH is present in this region of the eye (Fig. 3). Strong staining was observed in choroid vessels (retinal blood vessels) and in an area bordering the RPE. Drusen of similar composition to that found in AMD are found in the eyes of patients with membranoproliferative glomerulonephritis type II (MPGNII), a kidney disease (*30*); CFH deficiency can cause MPGNII (*23*). Our immunostaining experiments (Fig. 3 and fig. S1) suggest that in AMD, the risk variant of CFH may give rise to complement deposition in choroidal capillaries (more severe) and choroidal vessels (less severe), with subsequent leakage of plasma proteins into Bruch's membrane. Nutritional supplementation with zinc slows down the progression of AMD; biochemical studies have shown that CFH function is sensitive to zinc concentration (*12*, *31*).

We identified a tyrosine-histidine polymorphism in which the histidine variant almost always occurs in the context of the AMD risk haplotype. This polymorphism is located in a region of CFH that binds to both heparin and C-reactive protein (CRP) (*23*). It has been previously suggested that this binding could be altered by the replacement of a neutral tyrosine with a positively charged histidine (*23*). Elevated serum levels of CRP have been shown to be associated with AMD (*32*). Further work to establish the causal role of the tyrosine-histidine polymorphism in AMD is warranted.

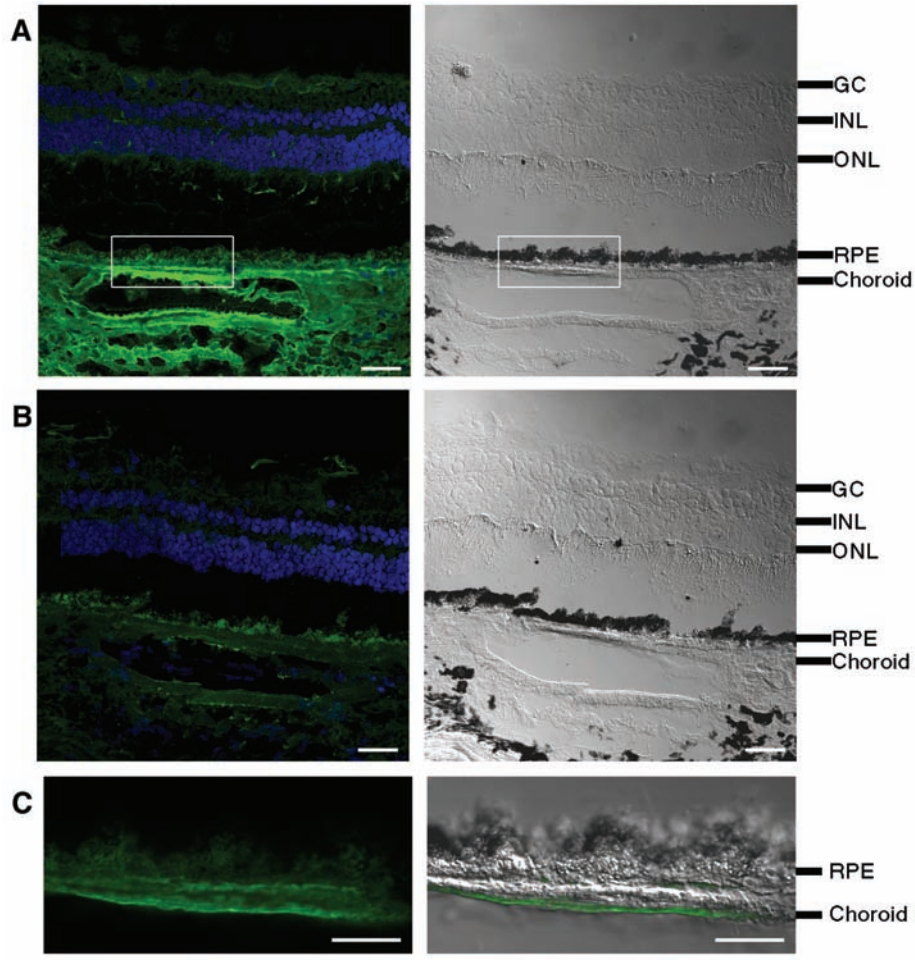

Fig. 3. Immunofluorescence localization of CFH protein in human retina. Neighboring human retina sections are stained with (**A**) antibody to CFH or (**B**) antibody to CFH preabsorbed with CFH as negative control. (**C**) High-magnification view of the boxed area in (A). For (A), (B), and (C), left panels are the fluorescence images, with CFH labeling in green and DAPI (4′,6′-diamidino-2-phenylindole)–stained nuclei in blue; right panels are differential interference contrast (DIC) images showing the tissue morphology. In (C), the CFH signal is superimposed onto the DIC image. Labeling of CFH is intense in choroid, including blood vessels and areas bordering RPE [(A) and (C)]; this CFH signal is competed away by purified CFH protein (B), which demonstrates the labeling specificity. The fluorescence signal from RPE arises from lipofuscin autofluorescence, which cannot be competed away with CFH protein [(A) and (B)]. The black spots in DIC images correspond to melanin granules in RPE and choroids. The cell layers are indicated: GC, ganglion cells; INL, inner nuclear layer; ONL, outer nuclear layer; RPE, retinal pigment epithelium. Scale bars: 40 μm in (A) and (B), 20 μm in (C).

References and Notes

1. D. S. Friedman *et al.*, *Arch. Ophthalmol.* **122**, 564 (2004).
2. J. Tuo, C. M. Bojanowski, C. C. Chan, *Prog. Retinal Eye Res.* **23**, 229 (2004).
3. AREDS Research Group, *Ophthalmology* **107**, 2224 (2000).
4. J. Majewski *et al.*, *Am. J. Hum. Genet.* **73**, 540 (2003).
5. J. M. Seddon, S. L. Santangelo, K. Book, S. Chong, J. Cote, *Am. J. Hum. Genet.* **73**, 780 (2003).
6. D. E. Weeks *et al.*, *Am. J. Hum. Genet.* **75**, 174 (2004).
7. G. R. Abecasis *et al.*, *Am. J. Hum. Genet.* **74**, 482 (2004).
8. S. K. Iyengar *et al.*, *Am. J. Hum. Genet.* **74**, 20 (2004).
9. N. Risch, K. Merikangas, *Science* **273**, 1516 (1996).
10. D. Botstein, N. Risch, *Nat. Genet.* **33** (suppl.), 228 (2003).
11. K. Ozaki *et al.*, *Nat. Genet.* **32**, 650 (2002).
12. AREDS Research Group, *Arch. Ophthalmol.* **119**, 1417 (2001).
13. Materials and methods are available as supporting material on *Science* Online.
14. L. M. McIntyre, E. R. Martin, K. L. Simonsen, N. L. Kaplan, *Genet. Epidemiol.* **19**, 18 (2000).
15. B. Devlin, S. A. Bacanu, K. Roeder, *Nat. Genet.* **36**, 1129 (2004).
16. Klein *et al.*, data not shown.
17. S. B. Gabriel *et al.*, *Science* **296**, 2225 (2002).

18. The International HapMap Consortium, *Nature* **426**, 789 (2003).
19. A. R. Templeton, E. Boerwinkle, C. F. Sing, *Genetics* **117**, 343 (1987).
20. D. W. Schultz *et al.*, *Hum. Mol. Genet.* **12**, 3315 (2003).
21. M. Hayashi *et al.*, *Ophthalmic Genet.* **25**, 111 (2004).
22. G. J. McKay *et al.*, *Mol. Vis.* **10**, 682 (2004).
23. S. Rodríguez de Cordoba, J. Esparza-Gordillo, E. Goicoechea de Jorge, M. Lopez-Trascasa, P. Sanchez-Corral, *Mol. Immunol.* **41**, 355 (2004).
24. L. V. Johnson, W. P. Leitner, M. K. Staples, D. H. Anderson, *Exp. Eye Res.* **73**, 887 (2001).
25. R. F. Mullins, S. R. Russell, D. H. Anderson, G. S. Hageman, *FASEB J.* **14**, 835 (2000).
26. J. Ambati *et al.*, *Nat. Med.* **9**, 1390 (2003).
27. G. S. Hageman *et al.*, *Prog. Retinal Eye Res.* **20**, 705 (2001).
28. J. Esparza-Gordillo *et al.*, *Immunogenetics* **56**, 77 (2004).
29. G. Wistow *et al.*, *Mol. Vis.* **8**, 205 (2002).
30. R. F. Mullins, N. Aptsiauri, G. S. Hageman, *Eye* **15**, 390 (2001).
31. A. M. Blom, L. Kask, B. Ramesh, A. Hillarp, *Arch. Biochem. Biophys.* **418**, 108 (2003).
32. J. M. Seddon, G. Gensler, R. C. Milton, M. L. Klein, N. Rifai, *JAMA* **291**, 704 (2004).
33. The Raymond and Beverly Sackler Fund for Arts and Sciences' generous support made this project possible. We thank Raymond Sackler, J. Sackler, and E. Vosburg for their input and encouragement. We also thank AREDS participants and investigators; G. Gensler, T. Clemons, and A. Lindblad for work on the AREDS Genetic Repository; S. Westman and A. Evan for assistance with the microarrays; R. Fariss for the human retinal sections and advice on confocal microscopy; E. Johnson for assistance with immunostaining; and J. Majewski for constructive comments on the manuscript. Partially funded by NIH-K25HG000060 and NIH-R01EY015771 (J.H.), Macula Vision Research Foundation and the David Woods Kemper Memorial Foundation (C.B.), NIH-R01MH44292 (J.O.), and NIH-K01RR16090 and Yale Pepper Center for Study of Diseases in Aging (C.Z.). This work also benefited from the International HapMap Consortium making their data available prior to publication.

Supporting Online Material
www.sciencemag.org/cgi/content/full/1109557/DC1
Materials and Methods
Fig. S1
Tables S1 to S5
References

10 January 2005; accepted 22 February 2005
Published online 10 March 2005;
10.1126/science.1109557
Include this information when citing this paper.

REPORTS

Quantum Phase Transition of a Magnet in a Spin Bath

H. M. Rønnow,[1,2,3]* R. Parthasarathy,[2] J. Jensen,[4] G. Aeppli,[5] T. F. Rosenbaum,[2] D. F. McMorrow[3,4,6]

The excitation spectrum of a model magnetic system, $LiHoF_4$, was studied with the use of neutron spectroscopy as the system was tuned to its quantum critical point by an applied magnetic field. The electronic mode softening expected for a quantum phase transition was forestalled by hyperfine coupling to the nuclear spins. We found that interactions with the nuclear spin bath controlled the length scale over which the excitations could be entangled. This generic result places a limit on our ability to observe intrinsic electronic quantum criticality.

The preparation and preservation of entangled quantum states is particularly relevant for the development of quantum computers, where interacting quantum bits (qubits) must produce states sufficiently long lived for meaningful manipulation. The state lifetime, typically referred to as decoherence time, is derived from coupling to the background environment. For solid-state quantum computing schemes, the qubits are typically electron spins, and they couple to two generic background environments (*1*). The oscillator bath—that is, delocalized environmental modes (*2*) such as thermal vibrations coupled via magnetoelastic terms to the spins—can be escaped by lowering the temperature to a point where the lattice is essentially frozen. Coupling to local degrees of freedom, such as nuclear magnetic moments that form a spin bath, may prove more difficult to avoid, because all spin-based candidate materials for quantum computation have at least one naturally occurring isotope that carries nuclear spin.

Experimental work in this area has been largely restricted to the relaxation of single, weakly interacting magnetic moments such as those on large molecules (*3*); much less is known about spins as they might interact in a real quantum computer. In this regard, the insight that quantum phase transitions (QPTs) (*4*) are a good arena for looking at fundamental quantum properties of strongly interacting spins turns out to be valuable, as it has already been for explorations of entanglement. In particular, we show that coupling to a nuclear spin bath limits the distance over which quantum mechanical mixing affects the electron spin dynamics.

QPTs are transitions between different ground states driven not by thermal fluctuations but by quantum fluctuations controlled by a parameter such as doping, pressure, or magnetic field (*5*, *6*). Much of the interest in QPTs stems from their importance for understanding materials with unconventional properties, such as heavy fermion systems and high-temperature superconductors. However, these materials are rather complex and do not easily lend themselves to a universal understanding of QPTs. To this end, it is desirable to identify quantum critical systems with a well-defined and solvable Hamiltonian and with a precisely controllable tuning parameter. One very simple model displaying a QPT is the Ising ferromagnet in a transverse magnetic field (*5*, *7*–*9*) with the Hamiltonian

$$\mathcal{H} = -\sum_{ij} \mathcal{J}_{ij}\, \sigma_i^z \cdot \sigma_j^z - \Gamma \sum_i \sigma_i^x \qquad (1)$$

where $\mathcal{J}_{ij}$ is the coupling between the spins on sites i and j represented by the Pauli matrices σ^z with eigenvalues ±1. In the absence of a magnetic field, the system orders ferromagnetically below a critical temperature T_c. The transverse-field Γ mixes the two states and leads to destruction of long-range order in a QPT at a critical field Γ_c, even at zero temperature. In the ferromagnetic state at zero field and temperature, the excitation spectrum is momentum independent and is centered at the energy $4\sum_j J_{ij}$ associated with single-spin reversal. Upon application of a magnetic field, however, the excitations acquire a dispersion, softening to zero at the zone center $q = 0$ when the QPT is reached.

We investigated the excitation spectrum around the QPT in $LiHoF_4$, which is an excellent physical realization of the transverse-field Ising model, with an added term accounting for the hyperfine coupling between electronic and nuclear moments (*10*–*12*). The dilution series $LiHo_xY_{1-x}F_4$ is the host for a wide variety of collective quantum effects, ranging from tunneling of single moments and domain walls to quantum annealing, entanglement, and Rabi oscillations (*13*–*17*). These intriguing properties rely largely on the ability of a transverse field, whether applied externally or generated internally by the off-diagonal part of the magnetic dipolar interaction, to mix two degenerate crystal field states of each Ho ion.

[1]Laboratory for Neutron Scattering, ETH-Zürich and Paul Scherrer Institut, 5232 Villigen, Switzerland. [2]James Franck Institute and Department of Physics, University of Chicago, Chicago, IL 60637, USA. [3]Risø National Laboratory, DK-4000 Roskilde, Denmark. [4]Ørsted Laboratory, Niels Bohr Institute fAPG, Universitetsparken 5, 2100 Copenhagen, Denmark. [5]London Centre for Nanotechnology and Department of Physics and Astronomy, University College London, London WC1E 6BT, UK. [6]ISIS, Rutherford Appleton Laboratory, Chilton, Didcot OX11 0QX, UK.

*To whom correspondence should be addressed. E-mail: henrik.ronnow@psi.ch